Searching for the optimal fluorophore in antimicrobial peptide sequences

Can Zhao,[1] Antonio Fernandez,[2] Nicolaos Avlonitis,[3] Greetje Vande Velde,[4] Mark Bradley,[3] Nick D. Read,[1,*] Marc Vendrell[2,*]

1 Manchester Fungal Infection Group, Institute of Inflammation and Repair, University of Manchester. CTF Building, Grafton St., M13 9NT Manchester, United Kingdom.

2 MRC Centre for Inflammation Research, The University of Edinburgh. 47 Little France Crescent, EH16 4TJ Edinburgh, United Kingdom.

3 EaStCHEM, School of Chemistry, The University of Edinburgh. West Mains Road, Edinburgh EH9 3FJ, United Kingdom.

4 Biomedical MRI Unit/MoSAIC, Department of Imaging and Pathology, KU Leuven, Leuven, Belgium.

KEYWORDS: fluorescence, labeling, imaging, probes, fungi, infection.

Abstract

With the advent of antimicrobial resistance, there is an urgent need for new strategies to treat infectious diseases. Antimicrobial peptides are considered as promising candidates, and therefore there is a need to understand their mechanism of action in order to exploit their therapeutic potential. To this end, fluorescent analogs are powerful tools to analyze their behavior and subcellular localization in cells and *in vivo*. However, the conjugation of fluorophores to antimicrobial peptides, especially in short sequences, can impair their biological activity, making the selection of the fluorescent label an essential step in these studies. In the present work, we have systematically modified a model antifungal hexapeptide with a collection of fluorophores covering broad physicochemical and spectral properties. The resulting conjugates have been examined in two different fungal species, in terms of their activity and intracellular localization. The biological results confirm the strong influence of the different fluorescent moieties on the properties of antimicrobial sequences, and provide an insight on the optimal fluorophores to be used in the preparation of fluorescent peptides for different bioimaging assays.

Introduction

In the past decades, fluorescent dyes have been broadly used as tags to visualize and study the roles of peptides in cells and *in vivo*.[1] For these studies, live cell imaging has become the technology of choice as it provides a direct readout of the localization of the peptides with high spatial and temporal resolution. In the context of antimicrobial peptides, several reports have described fluorescence labeling as an approach to study their mechanism of action[2-4] as well as to develop imaging probes for the rapid identification of microbes at infection sites.[5] In all cases, it is often assumed that fluorescently labeled peptides faithfully mimic the spatio-temporal dynamics of the native peptides, and fluorescent labels are typically chosen on the basis of excitation/emission wavelength, quantum yield, photobleaching, environmental sensitivity or chemical conjugation. Little attention has been paid to whether the fluorescent label might alter the physicochemical properties of the conjugate, and it is often unclear whether the fluorescent tag influences the uptake and localization of antimicrobial peptides inside the cells. In order to evaluate the impact that different fluorophores have in the biological properties of antimicrobial peptides and their application as imaging probes, we have synthesized a library of fluorescent conjugates based on the Peptide Antifungal 26 (PAF26), an antimicrobial sequence with high affinity for fungal cells.[6] In the present work, we have conjugated 12 different fluorophores (either in-house or commercially available) to the peptide sequence of PAF26 and compared their biological activity, cellular uptake and intracellular localization using live cell imaging. From these studies, we have observed that the activity of the conjugates is largely influenced by the fluorescent labels and that they accumulate in different intracellular regions depending on the fluorophore attached to the sequence. This systematic study will aid chemists working on

peptide-based imaging agents in the selection of the fluorophores for different fluorescence-based biological applications.

Results and Discussion

Design and synthesis of a library of fluorescent antifungal peptides

For many years, the synthesis of antimicrobial peptides has been widely adapted to combinatorial chemistry. However, libraries of antimicrobial peptides have been mainly focused on the optimization of the peptide sequences, either to enhance their antimicrobial activity, improve their selectivity against specific strains or pathogens, or to reduce their cytotoxicity in mammalian cells.[7-9] Some antimicrobial peptides have been labeled with fluorophores in order to visualize their localization in cells by confocal microscopy.[10] More recently, the high selectivity of antimicrobial sequences has been exploited to develop imaging contrast agents for the rapid identification of infection sites.[11,12] In most reports, only one fluorophore is employed on the basis of its compatibility with the experimental procedures. However, conventional fluorophores differ largely in their physicochemical features,[13,14] and therefore it is reasonable to expect that different fluorophores could induce variability on the activity and cellular localization properties of peptide sequences. For instance, Baker et al. reported the influence of different fluorescent labels in a combinatorial library of A_1R adenosine inhibitors, where significant differences were observed in the binding properties of several fluorescently-labeled inhibitors.[15] In the context of short antimicrobial peptides, there are no reports of any systematic evaluation of their biological properties after conjugation to various fluorescent labels. Herein, we have designed a library based on the antimicrobial peptide sequence PAF26, which was modified with a total of 12 fluorophores covering the whole spectral range (from blue to near-infrared emission) and diverse

physicochemical properties (Chart 1). In addition to conventional fluorophores (e.g. carboxyfluorescein, carboxyrhodamine, BODIPY, cyanine), we also included small fluorophores (e.g. NBD, dansyl), compounds with environmentally-sensitive properties (e.g. Nile Blue, malachite green, styryl), pH-sensitivity (e.g. naphthalimide) and esterase-activatable fluorophores (e.g. fluorescein diacetate). Overall, these fluorophores constitute a representative collection of the fluorescent labels that most chemists would employ for labeling any defined peptide sequence.

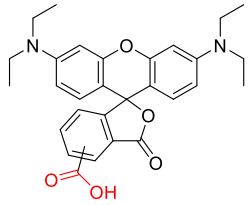

1

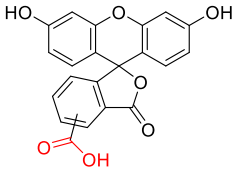

2

3

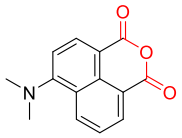

4

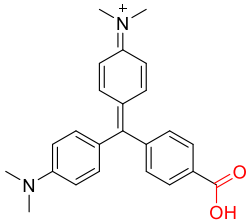

5

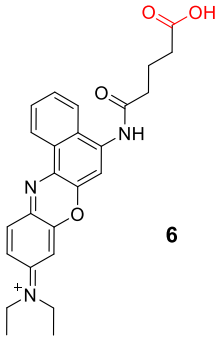

6

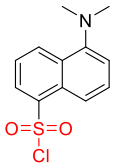

7

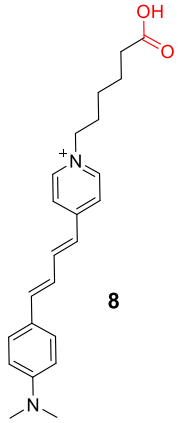

8

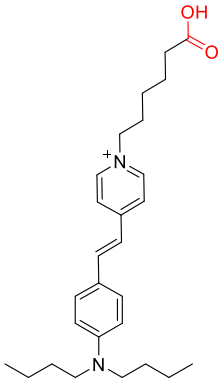

9

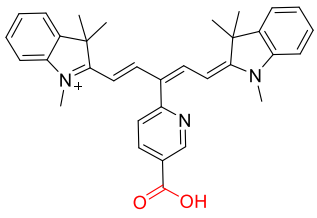

10

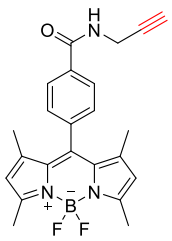

11

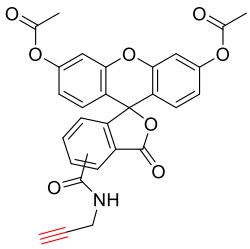

12

Chart 1. **Fluorescent labels for the derivatization of the antimicrobial peptide PAF26.** We employed 12 different fluorophores with suitable reactive groups (in red) for peptide labeling (e.g. carboxylic acids, sulfonyl chlorides, anhydrides, alkynes). Fluorophores **1**, **2**, **3** and **7** are commercially available, whereas the synthesis and characterization of all other fluorophores is described in the Experimental Procedures and the Electronic Supplementary Information (ESI).

PAF26 (H-RKKWFW-NH_2) is a short antimicrobial peptide with high affinity and selectivity for fungal cells over mammalian cells.[16] Like many other antimicrobial peptides, PAF26 contains both cationic and hydrophobic residues, and therefore it is an excellent model for examining the influence of fluorophores in the properties of antimicrobial peptides. We designed the synthesis of the hexapeptide using conventional solid-phase protocols in Rink amide polystyrene resin (Scheme 1). In order to incorporate suitable conjugation groups within the sequence of PAF26, we first synthesized two derivatives containing aminohexanoic or azidohexanoic spacers directly attached to the *N*-terminal group of PAF26. Through these spacers, fluorophores could be readily conjugated using their reactive groups (i.e., carboxylic acids, chlorides, anhydrides, sulfonyl chlorides or alkynes) without affecting the main recognition features of the antimicrobial peptide. Most library members were fully synthesized on solid support, including the coupling of the fluorophore, to render the final fluorescent PAF26 analogues upon acidic cleavage from the resin. Due to the lability of the fluorophores **11** and **12** (i.e., BODIPY and fluorescein diacetate, respectively) to acidic media, the corresponding derivatives **PAF26-11** and **PAF26-12** were prepared by 1,3-Huisgen dipolar cycloaddition using the azido-modified PAF26 and the fluorescent alkynes in solution phase (Scheme 1). All 12 fluorescent derivatives of PAF26 were purified by semi-preparative HPLC to isolate the final conjugates (**PAF26-1** to **PAF26-12**) in high purity (for characterization data, see ESI).

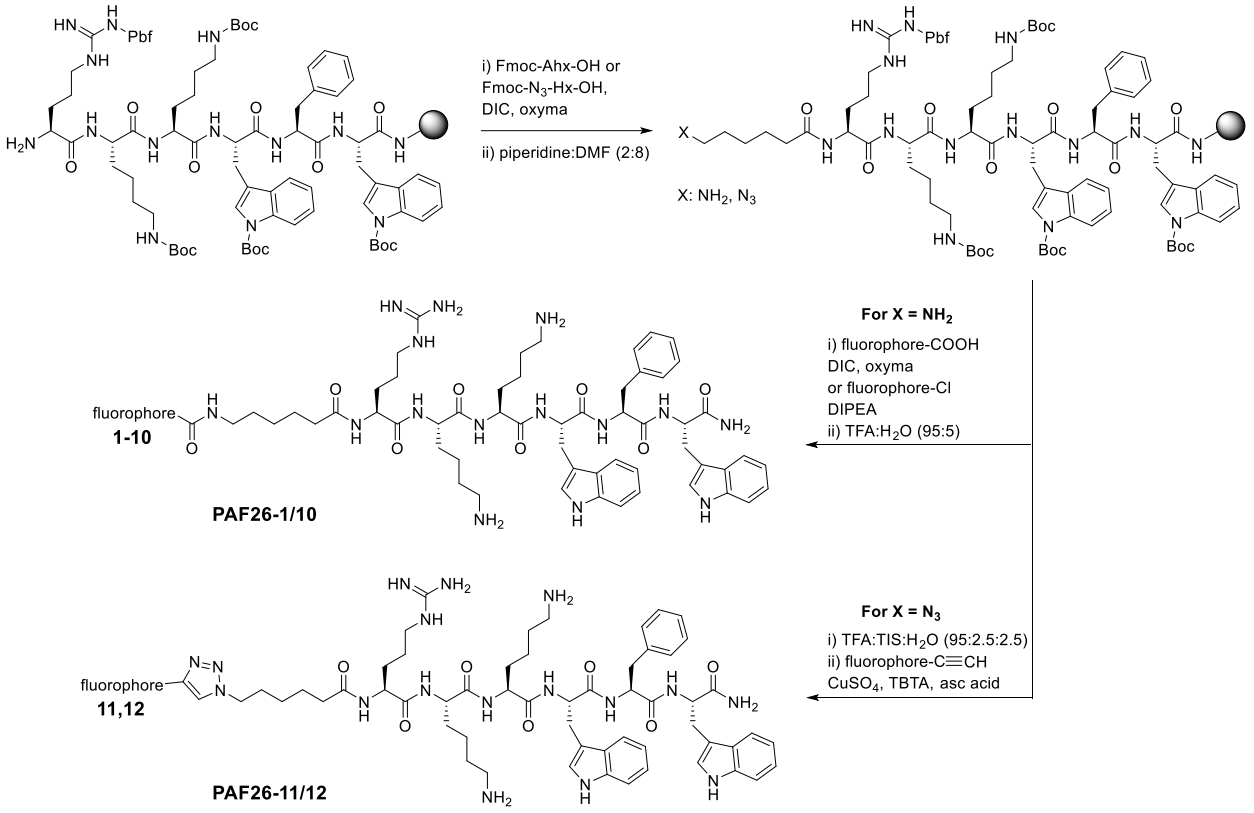

Scheme 1. Solid-phase synthesis of a library of fluorescent antimicrobial peptides based on the hexapeptide PAF26. The peptide sequence of PAF26 was modified with amino- or azidohexanoic spacers at the *N*-terminus to enable the conjugation of different fluorophores, either by formation of amide bonds in solid-phase or by 'click' chemistry in solution. All 12 conjugates **PAF26-1** to **PAF26-12** were isolated in good yields and high purities. For the chemical structures of the fluorophores **1-12**, see Chart 1.

In vitro biological activity of fluorescent antifungal peptides

After completing the synthesis of the library of fluorescent antimicrobial conjugates (**PAF26-1/12**), we measured their spectral properties and determined their IC_{50} values in two different fungal species (i.e., *Neurospora Crassa* and *Aspergillus Fumigatus*) as a measure of their cellular activity (Table 1). *N. Crassa* has been widely used as a model organism of filamentous fungi

whose genome has been entirely sequenced, whereas *A. fumigatus* is one of the most fatal fungal pathogens, able to cause invasive pulmonary Aspergillosis in immunosuppressed individuals.

Conjugates incorporating small fluorophores (e.g., NBD (**PAF26-3**), naphthalimide (**PAF26-4**), dansyl (**PAF26-7**)) did not show any significant differences in their antifungal activity when compared to the unlabeled sequence PAF26. This observation is in line with previous reports where NBD or dansyl have been described as highly tolerated fluorescence labels for the derivatization of biomolecules.[17] On the other hand, larger fluorophores showed a slight impairment in the antifungal activity of PAF26. A small improvement in activity was observed for positively-charged fluorophores, such as rhodamine, Nile Blue or styryl dyes (**PAF26-1**, **PAF26-6**, **PAF26-8** and **PAF26-9**, respectively), whereas fluorescein-based structures (**PAF26-2** and **PAF26-12**) exhibited slightly lower activity. From the library, two conjugates (**PAF26-10** and **PAF26-11**) stood out as antimicrobial peptides with significantly higher antifungal activity, showing around 2-fold lower IC_{50} values in both fungal species. The two corresponding fluorophores (i.e. cyanine (**10**) and BODIPY (**11**)) are highly cell permeable structures, which have been reported for the preparation of a range of fluorescent probes.[18-22] Altogether, these results corroborate the influence of the label in the biological properties of fluorescent PAF26 conjugates, where minimal impairment was observed for conjugates including small fluorophores and enhanced activity was found in sequences with cell permeable fluorophores.

Table 1. Spectral properties and biological activity of fluorescent antimicrobial sequences in fungal cells.

Compound	**$\lambda_{exc.}$ (nm)**	**$\lambda_{em.}$ (nm)**	**IC_{50} in *N. Crassa*‡**	**IC_{50} in *A. Fumigatus*‡**
PAF26	n.d.	n.d.	3.99 ± 0.67	7.99 ± 0.34
PAF26-1¥	563	593	3.82 ± 0.05	6.89 ± 0.16

PAF26-2[¥]	498	529	5.28 ± 0.15	9.11 ± 0.33
PAF26-3	488	552	4.41 ± 0.33	7.86 ± 0.09
PAF26-4	450	532	4.22 ± 0.20	8.01 ± 0.16
PAF26-5	635	n.d.	4.12 ± 0.42	9.66 ± 0.51
PAF26-6	635	679	3.22 ± 0.21	5.84 ± 0.18
PAF26-7	300	350	3.99 ± 0.07	7.87 ± 0.21
PAF26-8	465	706	3.01 ± 0.11	7.69 ± 0.13
PAF26-9	487	621	2.56 ± 0.19	7.21 ± 0.35
PAF26-10	633	660	1.96 ± 0.07	4.21 ± 0.39
PAF26-11	505	540	2.22 ± 0.21	3.72 ± 0.17
PAF26-12[¥]	503	530	5.34 ± 0.19	9.89 ± 0.37

[‡] Values (μM) represented as means ± s.e.m. (n=3).
[¥] Values obtained for the mixture of 5 and 6-carboxyisomers.

Fluorescence live cell imaging studies to analyze the localization of PAF26 conjugates in fungal cells

Next we performed live cell imaging experiments to examine the cellular uptake and intracellular localization of the different conjugates in *N. Crassa* and *A. fumigatus* by confocal laser scanning microscopy. Concentrations in the low micromolar range were used, as these have been previously optimized for the non-passive uptake of PAF26.[16] As shown in Fig 1, **PAF26-1** localized within the cell membrane structure and the vacuolar system of *N. crassa* conidial germlings, with rapid binding to the anionic cell membrane, partially favoured by the positive charge of the rhodamine fluorophore. In contrast, the carboxyfluorescein derivative **PAF26-2** showed a similar pattern of vesicular distribution but reduced staining on the cellular envelope due to its negatively charged structure (Fig. 1). The negative charge reduced the affinity of the conjugate for the cell envelope, with slower internalization and reduced cytotoxicity, in

accordance with the results obtained for the activity assays (Table 1). Similarly, the diacetylated derivative (**PAF26-12**) showed preferential staining of the vacuolar lumens with no fluorescence detected in the cellular membranes, being the fluorescence emission triggered only after the reaction with intracellular esterases (Fig. S1 in ESI). We performed co-localization experiments between **PAF26-12** and **PAF26-1** to observe that both conjugates displayed a similar cellular uptake, first appearing in small vesicles and then accumulating within the larger cell vacuoles (Fig. S2 in ESI).

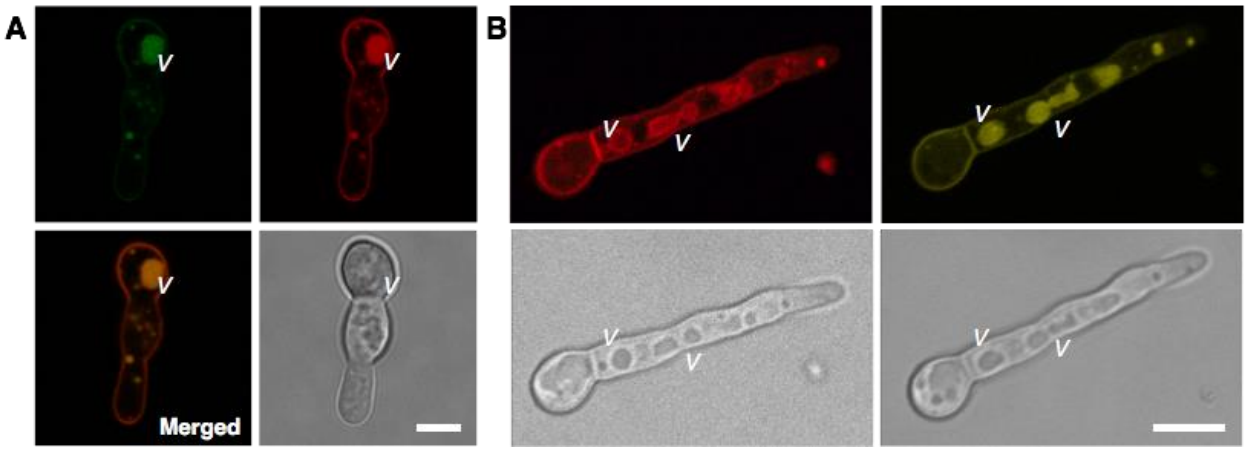

Figure 1. **Fluorescence microscope images of conidial germlings of *N. crassa* after incubation with PAF26-1, PAF26-2 or PAF26-8.** A) Fluorescence images of *N. crassa* after co-staining with **PAF26-1** (red, 0.5 μM) and **PAF26-2** (green, 0.5 μM) at 25 ºC. Scale bar: 2 μm; v: vacuole. B) Imaging of *N. crassa* after co-staining with **PAF26-8** (red, 1 μM) and **PAF26-1** (yellow, 1 μM) at 25 º C. Scale bar: 5 μm; v: vacuole.

Conjugates including small fluorophores, such as NBD (**PAF26-3**) or napthtalimide (**PAF26-4**), displayed similar intracellular vesicular localization, both in conidial germlings of *N. crassa* and *A. fumigatus* (Fig. S3 in ESI). Notably, the pH-sensitivity properties of **PAF26-4** enabled preferential imaging of acidified vesicular structures as opposite to the general vacuolar staining

observed with **PAF26-1** (Fig. S4 in ESI), opening the possibility to monitor intracellular pH changes in these subcellular structures. Conjugates including environmentally-sensitive fluorophores such as malachite green, Nile Blue or dansyl (**PAF26-5**, **PAF26-6** and **PAF26-7**) showed marginal staining in fungal cells, suggesting the potential accumulation of these sequences in neutral hydrophilic microenvironments (e.g. vacuoles), where these fluorophores exhibit very poor quantum yields.[23-24]

On the other hand, cationic styryl-based fluorophores (**PAF26-8** and **PAF26-9**) showed remarkably enhanced staining of the envelope of fungal cells. **PAF26-8** brightly stained the cellular membranes of *N. Crassa* at short time points to later internalize and accumulate in vesicles and vacuoles to a similar extent than **PAF26-1** (Fig. 1). Imaging experiments using **PAF26-9** also showed a similar behavior in both *N. Crassa* and *A. Fumigatus* (Fig. S5 in ESI). As observed for **PAF26-1**, the cationic character of the styryl fluorophores favoured the rapid interaction with anionic components of the cellular membranes and enhanced their internalization, with overall higher antifungal activities (Table 1). Interestingly, when we incubated **PAF26-8** with *A. fumigatus*, we did not observe any active transport into healthy cells, and hyphae were only stained by **PAF26-8** once the cell membrane structure was compromised (Fig. S6 and Movie S1 in ESI). These results highlight potential differences in the transport of **PAF26-8** between different fungal species, and suggest the possibility of using fluorescent labels as means to fine-tune the activity of antimicrobial sequences for specific species.

Finally, both cyanine and BODIPY-based conjugates (**PAF26-10** and **PAF26-11**, respectively) displayed a higher localization in the cytoplasm of fungal cells when compared to any other members of the library. The cyanine derivative (**PAF26-10**) brightly stained fungal cells and distributed in the membrane as well as in intracellular vacuoles and other regions of the

cytoplasm. Dual labeling experiments with the carboxyfluorescein derivative **PAF26-2** confirmed the presence of **PAF26-10** in subcellular vesicular organelles but also indicated its localization in other areas of the cytosol (Fig. 2). Likewise, the BODIPY derivative **PAF26-11** displayed homogeneous staining of the cytoplasm of fungal cells, with no specific accumulation in vacuoles or other subcellular organelles when co-localization experiments with **PAF26-1** were performed (Fig. 2). The combined analysis of the imaging and cytotoxicity data indicates that antimicrobial sequences labeled with cell permeable fluorophores (e.g. BODIPY, cyanine) displayed enhanced activity in fungal cells, and suggests that their preferential localization within the cytoplasm might be critical for their mode of action.

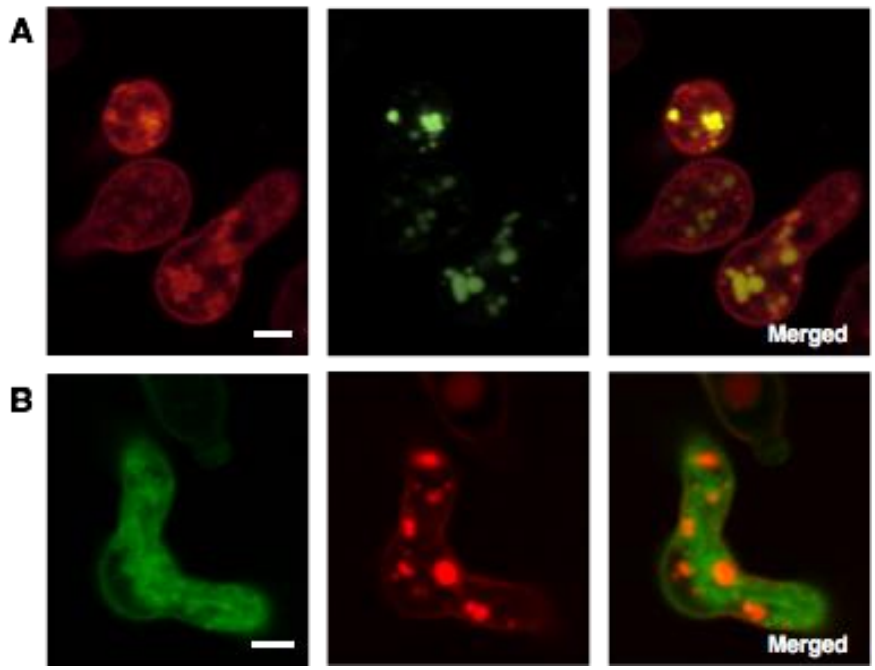

Figure 2. **Fluorescence microscope images of conidial germlings of *A. fumigatus* after incubation with PAF26-10 or PAF26-11.** A) Fluorescence images of *A. fumigatus* after co-staining with **PAF26-10** (red, 1 μM) and **PAF26-2** (green, 1 μM) at 37 ºC. Scale bar: 1 μm. B)

Fluorescence images of germinated *A. fumigatus* after co-staining with **PAF26-11** (green, 2 μM) and **PAF26-1** (red, 2 μM) at 37 °C. Scale bar: 1 μm.

Finally, in view of the bright staining of *A. fumigatus* upon incubation with **PAF26-10** (Figure 2A) and its fluorescence emission in the near-infrared region ($\lambda_{em.}$: 660 nm, Table 1), we assessed the suitability of **PAF26-10** for whole-body *in vivo* fluorescence imaging experiments in mice that had been infected with *A. fumigatus*. Near-infrared fluorophores are advantageous for *in vivo* imaging as the low autofluorescence background in such region of the spectra enhances the signal-to-noise ratios.[25-27] We determined the background and fluorescence signals in mice that had been treated with **PAF26-10**, and observed that the cyanine fluorophore was bright enough to provide a detectable signal from live animals using whole-body fluorescence imaging (Fig. S7 in ESI). These results are in good agreement with previous reports of cyanine-labeled peptides for *in vivo* imaging of cancer cells in xenograft models.[28,29]

Altogether, the systematic evaluation of a library of fluorescent PAF26-based antimicrobial peptides provided important clues of the optimal fluorophores for the preparation of fluorescent peptides and their application in bioimaging experiments. Whereas positively-charged structures (e.g. rhodamine, styryl) favor the interaction with the anionic membrane components, neutral (e.g. NBD) and negatively-charged fluorophores (e.g. fluorescein) preferentially accumulate in vacuoles, and pH-sensitive fluorophores (e.g. naphthalimide) offer the possibility of visualizing specific intracellular processes in real time, such as vacuolar acidification. Cell permeable fluorophores (e.g. cyanine) enhance the cellular activity of antimicrobial peptides, providing bright cytosolic staining and showing good discrimination from background signals in whole-body *in vivo* fluorescence imaging. These results confirm how fluorescent moieties influence the

biological properties of antimicrobial sequences and their non-negligible impact when designing fluorescence-based imaging assays.

Conclusions

Fluorescently labeled peptides are powerful tools for image-based mechanistic studies in cells. However, little is known on the influence of fluorescent tags in the uptake and localization of peptides inside the cells, and fluorophores are often selected only on the basis of their spectral properties. We have evaluated the impact of different fluorophores (either commercially available or synthetically accessible) in the biological properties of a model antimicrobial peptide by synthesizing a library of fluorescent derivatives of the antifungal hexapeptide PAF26. Solid-phase peptide synthesis followed by conventional amide formation or solution-phase 'click' conjugation for acid-sensitive fluorophores rendered a collection of 12 fluorescent conjugates with broad spectral and physicochemical properties. The assessment of the fluorescent peptides in two fungal species (*N. crassa* and *A. fumigatus*) indicated the strong influence of the fluorescent labels on both the antimicrobial activity and intracellular localization of the PAF26 peptide sequence, with small fluorophores having the most neutral effect and cell permeable dyes leading to enhanced activity and brightest intracellular staining. This systematic study will aid chemists working on peptide-based imaging agents in the selection of optimal fluorophores for various fluorescence-based biological applications.

Experimental Procedures

8-(Dimethylamino)-3-oxatricyclo[trideca-1,5,7,9,11-pentaene]-2,4-dione (4). 2.0 mL of dimethylamine aqueous solution (19.9 mmol) and a catalytic amount of $CuSO_4$ were added to a suspension of 4-bromo-1,8-naphthalenedicarboxylic anhydride (1.9 mmol) in DMF (50 mL). The mixture was then refluxed for 1.5 h, after which the solvent was evaporated under vacuum. Compound **4** was crystallized from ethanol as a yellow solid (275 mg, 57% yield). HPLC: t_R: = 4.74 min; MS (m/z): $[M+H]^+$ calcd for $C_{14}H_{11}NO_3$: 242.1; found: 242.2; ^{1}H NMR (500 MHz, DMSO-d_6): δ 8.59 (d, J = 8.4 Hz, 1H), 8.46 (d, J = 7.2 Hz, 1H), 8.32 (d, J = 8.4 Hz, 1H), 7.76 (t, J = 7.9 Hz, 1H), 7.20 (d, J = 8.4 Hz, 1H), 2.51 (s, 6H); ^{13}C NMR (126 MHz, DMSO-d_6): δ 162.0, 160.8, 157.8, 134.8, 133.6, 133.0, 125.5, 124.1, 119.3, 113.2, 108.4, 44.7.

***N*-(4-((4-carboxyphenyl)(4-(dimethylamino)phenyl)methylene)cyclohexa-2,5-dien-1-ylidene)-*N*-methylmethanaminium (5).** 4-(Bis(4-(dimethylamino)phenyl)methyl)benzoic acid (0.70 mmol) and *p*-chloranil (1.05 mmol) were dissolved in 30 mL $CHCl_3$, and 0.5 mL AcOH was added to the solution. The solution was stirred for 1.5 h at 35ºC. Compound **5** was crystallized in water to yield a green solid (176 mg, 70% yield). HPLC: t_R: = 4.28 min; MS (m/z): $[M^+]$ calcd for $C_{24}H_{25}N_2O_2^+$: 373.2; found: 373.2; ^{1}H NMR (500 MHz, DMSO-d_6) δ 10.21 (s, 1H), 8.14 (d, J = 8.4 Hz, 2H), 7.46 (d, J = 8.4 Hz, 2H), 7.35 (d, J = 9.4 Hz, 2H), 7.11 (d, J = 9.5 Hz, 2H), 6.98 (d, J = 9.0 Hz, 2H), 6.64 (d, J = 9.0 Hz, 2H), 3.31 (s, 6H), 3.06 (s, 6H); ^{13}C NMR (126 MHz, DMSO-d_6) δ 166.7, 157.0, 152.9, 151.6, 145.5, 144.6 (x 2), 140.5 (x 2), 132.7, 129.7, 128.9, 126.9 (x 2), 121.2 (x 2), 114.7 (x 2), 111.9 (x 2), 41.1 (x 2), 40.6 (x 2).

***N*-(5-(5-carboxybutanamido)-9*H*-benzo[a]phenoxazin-9-ylidene)-*N*-ethylethanaminium (6).** Nile Blue chloride (0.33 mmol) was dissolved in DCM together with glutaric anhydride (1 mmol) and DIPEA (1.14 mmol). The mixture was stirred at r.t. overnight. The crude mixture was then diluted with DCM and washed twice with water and then evaporated under vacuum. The

crude was then purified by column chromatography (DCM: MeOH, 9:1) to yield compound 6 as a dark blue solid (142 mg, 81% yield). HPLC: t_R: = 4.05 min; MS (m/z): [M^+] calculated for $C_{25}H_{26}N_3O_4^+$: 432.2; found: 432.2; ^{1}H NMR (500 MHz, DMSO-d_6) δ 8.75 (d, J = 8.0 Hz), 8.23 (s), 2.86 (q, J = 7.2 Hz), 2.35 (dt, J = 14.8 Hz, 4.6 Hz), 2.24 (t, J = 7.4 Hz), 1.93 – 1.77 (m), 1.71 (dd, J = 14.8 Hz, 7.4 Hz), 1.15 (d, J = 6.6 Hz); ^{13}C NMR (126 MHz, DMSO-d_6) δ 178.4, 174.6, 174.6, 164.2, 51.5, 33.3, 21.6, 21.3, 21.3, 20.5, 20.5, 19.1, 19.1, 18.9, 14.5, 14.5, 14.5, 12.3, 12.0.

1-(5-carboxypentyl)-4-((1*E*,3*E*)-4-(4-(Dimethylamino)phenyl)buta-1,3-dienyl)pyridin-1-ium bromide (8). 4-Methylpyridine (5.4 mmol) and ethyl 6-bromohexanoate (6.5 mmol) were dissolved in 20 mL of ACN, the mixture was refluxed at 90ºC overnight. 1-(6-ethoxy-6-oxohexyl)-4-methylpyridinium was precipitated in cold Et_2O:hexane (1:1) to yield a light brown solid (1.9 g, quantitative yield). HPLC: t_R: = 3.58 min; MS (m/z): [M^+] calcd for $C_{14}H_{22}NO_2^+$: 236.2; found: 236.2. 1-(6-ethoxy-6-oxohexyl)-4-methylpyridinium (1.6 mmol) and 3-(4-(dimethylamino)phenyl)acrylaldehyde (2 mmol) were dissolved in 10 mL of EtOH in a microwave reaction vessel, then pyrrolidine (1.6 mmol) was added to the solution. The mixture was irradiated under microwave for 10 min at 120 ºC, and the crude was purified by column chromatography (DCM: MeOH, 9:1) to yield 4-((1*E*,3*E*)-4-(4-(dimethylamino)phenyl)buta-1,3-dien-1-yl)-1-(6-ethoxy- 6-oxohexyl)pyridin-1-ium bromide as a red solid (853 mg, quantitative yield). The ethyl ester (0.25 mmol) was dissolved in 2 mL THF and 1 mL MeOH, mixed with LiOH (1.25 mmol) in water (1 mL) and stirred overnight at r.t. to yield the carboxylic acid which was used *in situ* without any further purification. Characterization data for the ester: HPLC: t_R: = 4.73 min; MS (m/z): [M^+] calcd for $C_{25}H_{33}N_2O_2^+$: 393.3; found: 393.4; ^{1}H NMR (500 MHz, DMSO-d_6) δ 8.80 (d, J = 6.9 Hz, 2H), 8.05 (d, J = 7.0 Hz, 2H), 7.87 – 7.77 (m, 2H), 7.48 (d, J = 8.9 Hz, 2H), 7.02 (d, J = 6.6 Hz, 2H), 6.78 – 6.71 (m, 2H), 4.05 (q, J = 7.1 Hz, 2H), 2.99 (s, 6H),

2.31 (td, *J* = 7.3, 2.1 Hz, 2H), 1.95 – 1.83 (m, 2H), 1.61 – 1.52 (m, 2H), 1.38 – 1.25 (m, 2H), 1.19 (t, *J* = 7.1 Hz, 2H), 1.17 (t, *J* = 7.1 Hz, 3H). ^{13}C NMR (126 MHz, DMSO) δ 173.2, 153.6, 151.6, 144.1, 142.7, 129.6, 124.0, 123.6, 123.2, 112.5, 60.2, 59.5, 53.6, 33.6, 30.6, 25.3, 24.2, 23.0, 14.6.

(*E*)-1-(5-carboxypentyl)-4-(4-(Dibutylamino)styryl)pyridin-1-ium bromide (9). (3*E*,5*E*)- 1-(6-ethoxy-6-oxohexyl)-4-methylpyridinium (1.6 mmol) and 4-(dibutylamino)benzaldehyde (2 mmol) were dissolved in 10 mL of EtOH in a microwave reaction vessel, then pyrrolidine (1.6 mmol) was added to the solution. The mixture was left to react under microwave irradiation for 10 min at 120ºC. The crude was purified by column chromatography (DCM: MeOH, 9:1) to yield (*E*)-4-(4-(dibutylamino)styryl)-1-(6-ethoxy-6-oxohexyl)pyridin-1-ium bromide as a purple solid (703 mg, quantitative yield). The ethyl ester (0.25 mmol) was dissolved in 2 mL THF and 1 mL MeOH, mixed with LiOH (1.25 mmol) in water (1 mL) and stirred overnight at r.t. to yield the carboxylic acid which was used *in situ* without any further purification. Characterization data for the ester: HPLC: t_R: = 5.76 min; MS (m/z): [M^+] calcd for $C_{29}H_{43}N_2O_2^+$: 451.3; found: 451.4. ^{1}H NMR (500 MHz, DMSO-d_6) δ 8.76 (d, *J* = 7.0 Hz, 2H), 8.05 (d, *J* = 7.1 Hz, 2H), 7.91 (d, *J* = 16.0 Hz, 1H), 7.57 (d, *J* = 8.9 Hz, 2H), 7.12 (d, *J* = 16.0 Hz, 1H), 6.74 (d, *J* = 9.1 Hz, 2H), 4.41 (t, *J* = 7.4 Hz, 2H), 4.05 (q, *J* = 7.1 Hz, 4H), 3.41 – 3.34 (m, 3H), 2.31 (td, *J* = 7.3, 1.6 Hz, 2H), 1.98 – 1.84 (m, 2H), 1.63 – 1.47 (m, 4H), 1.41 – 1.25 (m, 4H), 1.20 (t, *J* = 7.1 Hz, 3H), 1.17 (t, *J* = 7.1 Hz, 3H), 0.93 (t, *J* = 7.4 Hz, 6H).^{13}C NMR (126 MHz, DMSO) δ 173.2, 154.3, 150.4, 143.9, 142.8, 139.1, 131.0, 122.7, 122.2, 117.0, 112.0, 60.2, 59.3, 53.6, 50.3, 33.6, 30.6, 29.5, 25.3, 23.1, 20.1, 14.6.

2-((1*E*,3*Z*)-3-(5-carboxypyridin-2-yl)-5-((*E*)-1,3,3-trimethylindolin-2-ylidene)penta-1,3-dien-1-yl)-1,3,3-trimethyl-3*H*-indol-1-ium iodide (10). 3*H*-Indolium-2,3,3-tetramethyl iodide

(0.72 mmol), NaOAc (0.72 mmol) and 6-(1,3-dioxopropan-2-yl) nicotinic acid (0.36 mmol) were added to a microwave reaction vessel with 10 mL Ac_2O:AcOH (1:1). The mixture was then heated up to 160ºC under microwave irradiation for 0.5 h, after which the solvent was evaporated under vacuum. The crude was then purified using column chromatography (DCM:MeOH, 98:2 to 9:1) to yield compound **10** as a blue solid (144 mg, 80% yield). HPLC: t_R: = 4.72 min; MS (m/z): [M^+] calcd for $C_{33}H_{34}N_3O_2^+$: 504.3; found: 504.4; ^{1}H NMR (500 MHz, DMSO-d_6) δ 9.26 (d, *J* = 1.3 Hz, 1H), 8.44 (s, 1H), 8.41 (s, 1H), 8.40 (d, *J* = 2.2 Hz, 1H), 8.39 (d, *J* = 2.2 Hz, 1H), 7.65 (d, *J* = 7.4 Hz, 1H), 7.56 (d, *J* = 8.0 Hz, 1H), 7.42 (dd, *J* = 8.0, 1.2 Hz, 2H), 7.40 (d, *J* = 1.1 Hz, 3H), 7.28 (ddd, *J* = 7.4, 6.5, 1.9 Hz, 2H), 5.85 (d, *J* = 14.3 Hz, 1H), 3.39 (s, 6H), 1.76 (s, 12H). ^{13}C NMR (126 MHz, DMSO) δ 177.5, 152.8, 152.4, 141.4, 139.9, 135.3, 133.7, 131.7, 131.1, 129.3, 128.8, 126.9, 126.3, 123.4, 11.9, 101.4, 52.6, 32.1, 27.5.

4-(1,3,5,5,7,9-Hexamethyl-5*H*-4λ^4,5λ^4-dipyrrolo[1,2-*c*:2',1'-*f*][1,3,2]diazaborinin-10-yl)-*N*-(prop-2-yn-1-yl)benzamide (11). 2,4-Dimethylpyrrole (4.5 mmol) and 4-carboxybenzaldehyde (2 mmol) were dissolved in DCM under Ar. One drop of TFA was added and the solution was stirred at r.t. until complete consumption of the aldehyde. Then, a solution of 2,3-dichloro-5,6-dicyano-1,4-benzoquinone (2 mmol) in DCM was added, and the stirring continued for 10 min followed by addition of triethylamine (4 mL) and BF_3Et_2O (4 mL). After stirring for another 2 h the reaction mixture was washed with water and dried, then solvent was evaporated under vacuum. The carboxylic acid was then purified by column chromatography (DCM: MeOH, 95:5). The crude product was then concentrated and precipitated (AcOEt: hexane, 1:1) to yield a dark red oil (160 mg, 20 % yield). HPLC: t_R: = 5.81 min; MS (m/z): [M^+] calcd for $C_{20}H_{19}BF_2N_2O_2$: 368.2; found: 368.2. Then, the carboxylic acid (0.19 mmol) was dissolved with oxyma (0.57 mmol) in DCM and stirred for 5 min. DIC (1.14 mmol) was added and stirred for

another 2 min. Propargylamine (0.21 mmol) was then added and whole mixture was stirred at r.t. for 3 h. Compound **11** was isolated as a bright orange solid (17 mg, 22% yield over all steps). HPLC: t_R: = 5.80 min; MS (m/z): $[M+H]^+$ calcd for $C_{23}H_{22}BF_2N_3O$: 406.2; found: 406.2; ^{1}H NMR (500 MHz, DMSO-d_6) δ 8.05 (d, J = 8.4 Hz, 2H), 7.52 (d, J = 8.4 Hz, 2H), 6.20 (s, 2H), 5.76 (s, 1H), 4.09 (dd, J = 5.6, 2.5 Hz, 2H), 2.47 (s, 6H), 1.35 (s, 6H); ^{13}C NMR (126 MHz, DMSO) δ 165.7, 143.2, 135.8, 134.8, 130.9, 128.7, 122.0, 112.1, 111.6, 98.8, 73.4, 29.1, 14.7, 14.6.

3-Oxo-6-(prop-2-yn-1-ylcarbamoyl)-3*H*-spiro[isobenzofuran-1,9'-xanthene]-3',6'-diyl diacetate (12). 5,6-carboxyfluorescein diacetate (0.43 mmol) and oxyma (1.29 mmol) were dissolved in DCM and stirred for 5 min. Then DIC (2.58 mmol) was added to the mixture, stirred for 2 min and propargylamine (1.29 mmol) was added. The whole mixture was stirred at r.t. for 3 h then evaporated under vacuum. Compound **12** was purified by column chromatography (DCM: MeOH: AcOH, 98:1:1) to yield a yellow oil (175 mg, 82% yield); HPLC: t_R: = 5.36 min; MS (m/z): $[M+H]^+$ calcd for $C_{28}H_{19}NO_8$: 497.1; found: 497.8; ^{1}H NMR (500 MHz, DMSO-d_6) δ 9.31 (t, *J* = 5.5 Hz, 1H), 9.13 (t, *J* = 5.5 Hz, 1H), 8.54 (dd, *J* = 1.6, 0.7 Hz, 1H), 8.29 (dd, *J* = 8.1, 1.6 Hz, 1H), 8.22 (d, *J* = 1.4 Hz, 1H), 8.16 (dd, *J* = 8.1, 0.7 Hz, 1H), 7.83 (t, *J* = 1.0 Hz, 1H), 7.55 (dd, *J* = 8.0, 0.7 Hz, 1H), 7.37 – 7.28 (m, 2H), 7.02 – 6.90 (m, 6H), 4.12 (dd, *J* = 5.5, 2.5 Hz, 2H), 4.00 (dd, *J* = 5.5, 2.5 Hz, 2H), 3.16 (t, *J* = 2.5 Hz, 1H), 3.08 (t, *J* = 2.5 Hz, 1H), 2.29 (s, 3H), 2.29 (s, 3H).^{13}C NMR (126 MHz, DMSO) δ 170.3, 169.0, 167.4, 155.5, 152.4, 150.8, 135.5, 134.9, 130.0, 129.4, 119.1, 115.9, 110.6, 82.4, 81.4, 73.5, 29.6, 20.9.

Solid-phase peptide synthesis. All peptides were manually synthesized in polystyrene syringes fitted with a polyethylene porous disc using Fmoc-based SPPS. Solvents and soluble reagents were removed by suction. The Fmoc group was removed with piperidine: DMF (1:4) (1 × 1 min,

2 × 10 min). Peptide synthesis transformations and washings were performed at r.t. For peptide elongation, after the Fmoc group was removed, resins were washed with DMF (4 × 1 min), DCM (3 × 1 min) and DMF (4 x 1 min). Unless otherwise noted, standard coupling procedures were used with DIC (3 eq.) and OxymaPure (3 eq.) in DMF for 1-2 h and 5-min of pre-activation. The completion of the coupling was monitored by the Kaiser test.[30] Then, resins were filtered and washed with DCM (4 x 1 min) and DMF (4 x 1 min).

Synthesis of the peptides PAF26-1/10. For conjugates **PAF26-1**, **PAF26-2**, **PAF26-5**, **PAF26-6**, **PAF26-8**, **PAF26-9**, **PAF26-10**, standard amide bond formation coupling conditions with fluorophore-COOH (3 eq.), DIC (3 eq.) and OxymaPure (3 eq.) in DMF were used. For compounds **PAF26-3**, **PAF26-4** and **PAF26-7**, coupling of the dyes was accomplished by incubation of the peptide with the fluorophore (3 eq.) and DIPEA (3 eq.) in DMF. All resins were then washed with DMF (4 × 1 min) and DCM (3 × 1 min). For the cleavages, resins were stirred in 5 mL of TFA: H_2O (95:5) for 2 h at r.t. The beads were washed with TFA thoroughly and the peptides precipitated with ice-cold Et_2O after rotary evaporation before final purification by semi-preparative HPLC. Characterization details can be found in the ESI.

Synthesis of the peptides PAF26-11/12. Azido-derivatized peptides were cleaved from the resin by cleavage with 5 mL of TFA: H_2O: TIS (95:2.5:2.5) for 2 h at r.t. The beads were washed with TFA thoroughly and the peptides precipitated with ice-cold Et_2O after rotary evaporation. For the conjugation was performed, the peptide (1 eq.), ascorbic acid (1 eq.), tris[(1-benzyl-1*H*-1,2,3-triazol-4-yl)methyl] amine (TBTA) (0.3 eq.) and $CuSO_4$ (0.3 eq.) were dissolved in H_2O, and the corresponding alkynes (2 eq.) were added using a minimum amount of MeOH, leaving the reaction for aprox. 4 h at r.t. The reaction was monitored with HPLC, and upon completion,

peptides were purified by semi-preparative HPLC. Characterization details can be found in the ESI.

Measurement of spectral properties. Spectroscopic data were recorded on a Synergy HT spectrophotometer (Biotek). Compounds were dissolved at concentrations around 10 μM-50 μM in phosphate buffer saline (PBS) and spectra were recorded at r.t.

Cultures of *Neurospora Crassa*. *N. crassa* was grown at 25 °C in an incubator under constant artificial light. For conidial cultures, the strains were inoculated on small (35 x 10 mm) Vogel's medium plates[31] and incubated for 5 days. Conidia were harvested from cultures on days 5 to 7. *N. crassa* conidia were harvested from the plates in sterile dH_2O by washing 1 mL repeatedly over the culture surface. The resulting suspension was then filtered through a triple layer of Miracloth to remove any fragments of hyphae. The suspension was then vortexed vigorously to separate conidia and ensure even distribution. 10 μL of the suspension was mixed with 990 μL dH_2O and the conidial density determined using a haemocytometer.

Cultures of *Aspergillus Fumigatus*. *A. fumigatus* strains were grown on Vogel's medium at 37°C for 7 days. Conidia were collected in 0.05% Tween 80 by gently scraping a spatula over the fungal colony surface. The suspension was then passed through autoclaved Miracloth to remove any hyphal residues and stored at 4°C.

Antimicrobial activity measurements. Peptides at different concentrations were mixed with *N. Crassa* or *A. fumigatus* conidia to reach a final volume of 100 μL per well and a final conidial concentration of 5×10^5 cells/mL in 10% Vogel's medium. The BacTiter-Glo™ Microbial Cell Viability Assay kit (Promega) and CELLSTAR white polystyrene flat bottomed 96-well plates (Greiner) were used for these assays. After 24 h incubation (at 25 °C for *N. Crassa* or 37 °C for *A. fumigatus*), fungal growth was determined by measurement of the luminescence in a TriStar

LB 941 Multimode microplate reader. IC_{50} values were determined using four parameter logistic regression. Data analysis was performed using Sigma Plot 10.0. Values are represented as means ± s.e.m. from two independent experiments (n = 3).

Confocal live cell microscopy. *N. crassa* for confocal live cell imaging was grown on 100% Vogel's agar medium at 25 ºC for 3-5 days before the spores were harvested. The *A. fumigatus* CEA10 strain used for confocal live cell imaging was grown on 100% Vogel's medium at 37 ºC for 4-5 days before the spores were harvested. *N. crassa* spores were incubated in 8-well chambers for 3 h at 25 ºC in 10% Vogel's medium, and *A. fumigatus* spores were incubated for 16 h at 37 ºC in 10% Vogel's medium in order to allow germination. Live cell imaging of germinated fungi spores was performed using a Leica TCS SP8 confocal laser scanning microscope equipped with photo multiplier tubes, hybrid GaAsP detectors and a 63× water immersion objective. White light (450-750 nm), Ar (458 nm, 476 nm, 488 nm and 496 nm) and UV lasers (405 nm) were used for excitation. Images were processed and analyzed using Imaris scientific 3D/4D image processing and the analysis software 8.0 developed by Bitplane (Zurich, Switzerland). Details on the excitation and emission filters used for all the **PAF26-1/12** conjugates can be found in the ESI.

In Vivo Fluorescence Imaging. Animal experiments were carried out in compliance with national and European regulations and were approved by the animal ethics committee of KU Leuven (p103−2012). 9-Week-old female Balb/C mice of (Balb/cAnNCrl from Charles River Laboratories, bred at the KU Leuven animal facility, Leuven, Belgium) were kept in individually ventilated cages with free access to food and water. Immune competent mice (n = 3) were infected by inhalation of a fungal yeast cell suspension (Cryptococcus gattii R265, 50 000 CFUs in 20 μL of PBS, 10 μL per nostril) under transient isoflurane gas anesthesia (2% in pure O2).

Three weeks after infection, whole-body fluorescence imaging was carried out under isoflurane anesthesia on an IVIS Spectrum system with Living Image software (version 4.5.2, PerkinElmer). The fluorescence signal intensity was measured using the excitation/emission 640/680 filter pair before and 5 min after intratracheal administration of 7.5 nmol of the PAF26-10 derivative.

Supporting Information. NMR spectra and additional characterization data for the fluorescent PAF26 conjugates, additional imaging data. This material is available free of charge via the Internet at http://pubs.acs.org.

Author Information

The manuscript was written through contributions of all authors. All authors have given approval to the final version of the manuscript.

* Corresponding authors: nick.read@manchester.ac.uk; marc.vendrell@ed.ac.uk

Acknowledgements

A.F. acknowledges the funding from the Foundation Alfonso Martin Escudero (FAME, Spain). M. V. acknowledges funding from the Medical Research Council and the Marie Curie Career Integration Grant (333487).

Abbreviations

PAF26, Peptide Antifungal 26; NBD-Cl, 4-chloro-7-nitro-2,1,3-benzoxadiazole; BODIPY, 4,4-difluoro-4-bora-3a,4a-diaza-s-indacene; TFA, trifluoroacetic acid; DIC, diisopropylcarbodiimide; DCM, dichloromethane, TBTA, tris(benzyltriazolylmethyl)amine.

References

[1] González-Vera, J.A. Probing the kinome in real time with fluorescent peptides. *Chem. Soc. Rev.* **2012**, *41*, 1652-1664.

[2] Mania, D.; Hilpert, K.; Ruden, S.; Fischer, R.; Takeshita, N. Screening for antifungal peptides and their modes of action in Aspergillus nidulans. *Appl. Environ. Microbiol.* **2010**, *76*, 7102-7108.

[3] Maurya, I.K.; Pathak, S.; Sharma, M.; Sanwal, H.; Chaudhary, P.; Tupe, S.; Deshpande, M.; Chauhan, V.S.; Prasad, R. Antifungal activity of novel synthetic peptides by accumulation of reactive oxygen species and disruption of cell wall against Candida albicans. *Peptides* **2011**, *32*, 1732-1740.

[4] Binder, U.; Bencina, M.; Eigentler, A.; Meyer, V.; Marx, F. The Aspergillus giganteus antifungal protein AFPNN5353 activates the cell wall integrity pathway and perturbs calcium homeostasis. *BMC Microbiol.* **2011**, *11*, 209.

[5] Mendive-Tapia, L.; Zhao, C.; Akram, A.R.; Preciado, S.; Albericio, F.; Lee, M.; Serrels, A.; Kielland, N.; Read, N.D.; Lavilla, R.; Vendrell, M. Spacer-free BODIPY fluorogens in antimicrobial peptides for direct imaging of fungal infection in human tissue. *Nat. Commun*. **2016**, *7*, 10940 (DOI: 10.1038/ncomms10940).

[6] Lopez-Garcia, B.; Perez-Paya, E.; Marcos, J. F. Identification of novel hexapeptides bioactive against phytopathogenic fungi through screening of a synthetic peptide combinatorial library. *Appl. Environ. Microbiol.* **2002**, *68*, 2453–2460.

[7] Sudheendra, U.S.; Dhople, V.; Datta, A.; Kar, R.K.; Shelburne, C.E.; Bhunia, A.; Ramamoorthy, A. Membrane disruptive antimicrobial activities of human b-defensin-3 analogs. *Eur. J. Med. Chem.* **2015**, *91*, 91-99.

[8] Torcato, I.M.; Huan, Y.H.; Franquelim, H.G.; Gaspar, D.; Craik, D.J.; Castanho, M.A.; Troeira Henriques, S. Design and characterization of novel antimicrobial peptides, R-BP100 and RW-BP100, with activity against Gram-negative and Gram-positive bacteria. *Biochim. Biophys. Acta* **2013**, *1828*, 944-955.

[9] Gee, M.L.; Burton, M.; Grevis-James, A.; Hossain, M.A.; McArthur, S.; Palombo, E.A.; Wade, J.D.; Clayton, A.H. Imaging the action of antimicrobial peptides. *Sci. Rep.* **2013**, 3, 1557.

[10] Scheinpflug, K.; Krylova, O.; Nikolenko, H.; Thurm, C.; Dathe, M. Evidence for a novel mechanism of antimicrobial action of a cyclic R-, W-rich hexapeptide. *PLoS One* **2015**, *10*, e0125056.

[11] Welling, M.M.; Bunschoten, A.; Kuil, J.; Nelissen, R.G.H.H.; Beekman, F.J.; Buckle, T.; van Leeuwen, F.W.B. Development of a hybrid tracer for SPECT and optical imaging of bacterial infections. *Bioconjugate Chem.* **2015**, *26*, 839–849.

[12] Akram, A.R.; Avlonitis, N.; Lilienkampf, A.; Perez-Lopez, A.M.; McDonald, N.; Chankeshwara, S.V.; Scholefield, E.; Haslett, C.; Bradley, M.; Dhaliwal, K. A labelled-ubiquicidin antimicrobial peptide for immediate in situ optical detection of live bacteria in human alveolar lung tissue. *Chem. Sci.* **2015**, *6*, 6971–6979.

[13] Stockert, J.C.; Abasolo, M.I.; Blazquez-Castro, A.; Horobin, R.W.; Revilla, M.; Lombardo, D.M. Selective labelling of lipid droplets in aldehyde fixed cell monolayers by lipophilic fluorochromes. *Biotech. Histochem*. **2010**, *85*, 277-283.

[14] Vendrell, M.; Zhai, D.; Er, J.C.; Chang, Y.T. Combinatorial strategies in fluorescent probe development. *Chem. Rev.* **2012**, *112*, 4391-4420.

[15] Baker, J.G.; Middleton, R.; Adams, L.; May, L.T.; Briddon, S.J.; Kellam, B.; Hill, S.J. Influence of fluorophore and linker composition on the pharmacology of fluorescent adenosine A1 ligands. *Br. J. Pharmacol.* **2010***, 159*, 772-786.

[16] Muñoz, A.; Marcos, J.F.; Read, N.D. Concentration-dependent mechanisms of cell penetration and killing by the de novo designed antifungal hexapeptide PAF26. *Mol. Microbiol,* **2012**, *85*, 89-106.

[17] Jansenn, M.J.; Ensing, K.; de Zeeuw, R.A. Fluorescent-labeled ligands for the benzodiazepine receptor. Part 2: The choice of an optimal fluorescent-labeled ligand for benzodiazepine receptor assays. *Pharmazie* **2000**, *55*, 102-106.

[18] Lee, J.S.; Kang, N.Y.; Kim, Y.K.; Kim, H.K.; Samanta, A.; Feng, S.; Vendrell, M.; Park, J.H.; Chang. Y.T. Synthesis of a BODIPY library and its application to the development of live cell glucagon imaging probe. *J. Am. Chem. Soc*. **2009**, *131*, 10077-10082.

[19] Vendrell, M.; Samanta, A.; Yun, S.W.; Chang, Y.T. Synthesis and characterization of a cell-permeable near-infrared fluorescent deoxyglucose analogue for cancer cell imaging. *Org. Biomol. Chem.* **2011**, *9*, 4760-4762.

[20] Zhai, D.; Lee, S.C.; Vendrell, M.; Leong, L.P.; Chang, Y.T. Synthesis of a novel BODIPY library and its application in the discovery of a fructose sensor. *ACS Comb. Sci.* **2012**, *14*, 81-84.

[21] Er, J.C.; Vendrell, M.; Tang, M.K.; Zhai, D.; Chang, Y.T. Fluorescent dye cocktail for multiplex drug-site mapping on human serum albumin. *ACS Comb. Sci.* **2013**, *15*, 452-457.

[22] Rimpelova, S.; Briza, T.; Kralova, J.; Zaruba, K.; Kejik, Z.; Cisarova, I.; Martasek, P.; Ruml, T.; Kral, V. Rational design of chemical ligands for selective mitochondrial targeting. *Bioconjugate Chem*. **2013**, *24*, 1445-1454.

[23] Tajalli, H.; Gilani, A.G.; Zaherhamidi, M.S.; Tajalli, P. The photophysical properties of Nile red and Nile blue in ordered anisotropic media. *Dyes Pigments* **2008**, *78*, 15-24.

[24] Loving, G.S., Sainlos, M., Imperiali, B. Monitoring protein interactions and dynamics with solvatochromic fluorophores. *Trends Biotechnol.* **2010**, *28*, 73–83.

[25] Frangioni, J.V. In vivo near-infrared fluorescence imaging. *Curr. Opin. Chem. Biol*. **2003**, *7*, 626-634.

[26] Vendrell, M., Samanta, A., Yun, S.W., Chang, Y.T. Synthesis and characterization of a cell-permeable near-infrared fluorescent deoxyglucose analogue for cancer cell imaging. *Org. Biomol. Chem.* **2011**, *9*, 4760-4762.

[27] Samanta, A., Vendrell, M., Yun, S.W., Guan, Z., Xu, Q.H., Chang, Y.T. A photostable near-IR protein labeling dye for in vivo imaging. *Chem. Asian J.* **2011**, *6*, 1353-1357.

[28] Xin, J., Zhang, X., Liang, J., Xia, L., Yin, J., Nie, Y., Wu, K., Tian, J. In vivo gastric cancer targeting and imaging using novel symmetric cyanine dye-conjugated GX1 peptide probes. *Bioconjugate Chem.* **2013**, *24*, 1134-1143.

[29] Kim, E.M., Park, E.H., Cheong, S.J., Lee, C.M., Jeong, H.J., Kim, D.W., Lim, S.T., Sohn, M.H. In vivo imaging of mesenchymal-epithelial transition factor (c-Met) expression using an optical imaging system. *Bioconjugate Chem.* **2009**, *20*, 1299-1306.

[30] Kaiser, E., Colescott, R. L., Bossinger C. D., Cook, P. I. Color test for detection of free terminal amino groups in the solid-phase synthesis of peptides. *Anal. Biochem*. **1970**, 34, 595-598.

[31] Vogel, H. J. A convenient growth medium for Neurospora (Medium N). *Microbial Genet. Bull*. **1956**, 13, 42-43.

Table of Contents Graphic

Not just a pretty color. The synthesis and systematic evaluation of a library of fluorescent antimicrobial sequences provides new insights on the fluorophores of choice for different bioimaging applications.